Antifungal Mechanism of $[Ru^{III}(NH_3)_4catechol]^+$ Complex on Fluconazole-Resistant *Candida tropicalis*

Rafael Araújo Gomes-Junior[a], Roberto Santana da Silva[b], Renata Galvão de Lima[c], Marcos A. Vannier-Santos[a1]

[a]*Gonçalo Moniz Institute, Oswaldo Cruz Foundation (FIOCRUZ), Salvador, BA, Brazil;* [b]*Faculdade de Ciências Farmacêuticas de Ribeirão Preto, Universidade de São Paulo, Av. do Café s/n, 14040-903, Ribeirão Preto, SP, Brazil.,* [c]*Faculdade de Ciências Integradas do Pontal, Universidade Federal de Uberlândia, Rua Vinte, 1600, Tupã, Ituiutaba, MG, Brazil.*

1- Corresponding author: Dr. Marcos André Vannier-Santos
Laboratório de Biologia Parasitária, Instituto Gonçalo Moniz; Fundação Oswaldo Cruz – FIOCRUZ; Rua Waldemar Falcão, 121 Brotas, Salvador, Bahia, Brazil CEP 40295-00, Phone: +55-071-31762208. Emails: vannier@bahia.fiocruz.br or marcos.vannier@pesquisador.cnpq.br

Abstract

Candidiasis, a major opportunistic mycosis caused by *Candida* sp. may comprise life-threatening systemic infections. The incidence of non-*albicans* species is rising, particularly in South America and they are frequently drug resistant, causing unresponsive cases. Thus, novel antimycotic agents are required. Here we tested the antifungal activity of $[Ru^{III}(NH_3)_4catechol]^+$ complex (RuCat), approaching possible action mechanisms on fluconazole-resistant *Candida tropicalis*. RuCat significantly ($p<0.05$) inhibited the growth and viability of *C. tropicalis* dose-dependently, (IC_{50} 20.3µM). Cytotoxicity of RuCat upon murine splenocytes was lower (Selectivity Index = 16). Scanning electron microscopy analysis showed pseudohyphae formation, yeast aggregation and surface damage. RuCat-treated samples investigated by transmission electron microscopy showed melanin granule trafficking to cell surfaces and extracellular milieu. Surface adherent membrane fragments and extracellular debris were also observed. RuCat treatment produced intense H_2DCFDA labeling, indicating reactive oxygen species (ROS) production which caused increased lipoperoxidation. ROS are involved in the fungicidal effect as *N*-acetyl-L-cysteine completely restored cell viability. Calcofluor White chitin staining suggest that 70 or 140 µM RuCat treatment for 2h affected cell wall structure. PI labeling indicated necrotic cell death. The present data indicate that RuCat triggers ROS production, lipoperoxidation and cell surface damage, culminating in selective necrotic death of drug-resistant *C. tropicalis.*

Keywords: *Candida tropicalis*, fluconazole-resistant, ruthenium complex, catechol, antifungal agents, candidiasis

Introduction

Candida genus includes about 350 species found in humans among other mammals (Nunn *et al.* 2007). Candidiasis is an opportunistic infection increased over the last decades (Ghannoum 2001; Melo *et al.* 2004). Despite its diversity, few species (*C. albicans*, *C. glabrata*, *C. tropicalis*, *C. krusei*, *C. parapsilosis*, *C. kefyr*, *C. guilliermondii*, *C. pseudotropicalis*, *C. dubliniensis* and *C. lusitaniae*) are implicated in human disease.

C. albicans is a common pathogen found in the microbiome of the skin, gastrointestinal mucosa and human cavities. The spectrum of diseases caused by *Candida* ranges from oral candidiasis to life-threatening systemic infections. Immunocompromising conditions significantly promote the fungal spread (Gudlaugsson *et al.* 2003; Moran *et al*. 2012). Microbiome changes, gastrointestinal mucosa injury, chemotherapy, intestinal obstruction, prolonged fasting, parenteral nutrition and hypotension potentiate the mesenteric capillaries colonization by *Candida* sp., leading to candidemia (Takahashi *et al.* 2003).

Increased invasive fungal infections are often caused by *Candida* sp. (Warnock 2007), are associated with 30% and 50% mortality rates among children and adults respectively (Oliveira *et al.* 2014). Non-*albicans* species were reported, to cause 50% of the invasive infections (Ruiz *et al.* 2005; García-Rodríguez *et al.* 2013). *C. tropicalis* is the second/third non-*albicans* causative agent of bloodstream infections (Cantón *et al*. 2001; Colombo and Guimarães 2003). Moreover, these infections are more invasive and often chemotherapy unresponsive (Cantón *et al.* 2001; Morace *et al.* 2011), mainly in Latin America (Nucci *et al.* 2010).

Candidiasis treatment usually employs azole derivatives, as fluconazole, miconazole, itraconazole, however azole-resistant isolates are occurring more frequently (Canuto and Rodero 2002), so comprise a matter of concern. Thus, it is necessary to develop new strategies to prevent the spread of these fungi, so new antifungal drugs are required.

Catechols are phenolic compounds commonly found in nature and play a pivotal role in neurotransmission, taking part in the catecholamine structure. Phenolic allelochemicals as catechol and pyrogallol may be microbicidal upon both bacteria and fungi (Kocac and Ismet 2006). Redox reactions involving catechols in the presence of oxygen play important roles such as antimicrobial activity (Schweigert *et al*. 2001) mediated by reactive oxygen species (ROS).

From this perspective, the synergism by combining a ruthenium (III) ion and catechol ligand, as $[Ru^{III}(NH_3)_4(catechol)]^+$ complex (RuCat), was shown to alter the redox behavior as compared to free catechol (de Lima *et al.* 2003; 2004; Almeida *et al.* 2007). The coordination of the ruthenium (III) ion enhances oxygen consumption rates indicating that the reaction of the complex with oxygen is more thermodynamically favored facilitating the ROS production (Almeida *et al.* 2007).

Here we evaluated the RuCat antifungal activity against fluconazole-resistant *Candida tropicalis*.

Materials and methods

Apparatus for Ruthenium Complex Characterization

The ultraviolet-visible (UV-vis.) spectra were recorded Varian Cary 50 Conc. Infrared (IR) spectra were recorded on a Protegé 460 series FT-IR spectrometer, using solid samples pressed in KBr pellets. Chromatography was carried out in a Shimadzu system using a UV–vis. SPD- M20A detector, a LC-20AT pump with CBM-10A interface, a DGU-20A3 degasser and Chemstation software. A CLC-ODS column (5 µm; 250 mm 9 4, 6 mm i.d.; Shimadzu) was used. Samples were dissolved in the appropriate mobile phase, and 20 µL injection.

Chemicals and Reagents

$RuCl_3.3H_2O$, hydrazines and catechol were acquired as high purity reagents from Aldrich Chemicals (Brazil) and were used as supplied. All preparations and measurements were performed protected from light. Other chemicals were of reagent grade, so used without further purification.

$[Ru^{III}(NH_3)_4(catechol)](PF_6)$ complex synthesis

$[Ru^{III}(NH_3)_4(catechol)](PF_6)$ complex was synthesized as previously described (da Silva *et al.* 2000). The purity of the complexes was checked by HPLC analysis (Suppl. Figure 1), characterized by UV-vis. and IR spectroscopy and compared to published results (Santana da Silva *et al.* 2000). UV-vis. spectra: λ (nm) $[Ru^{III}(NH_3)_4(catechol)]^+$: 280 and 670 and FTIR ν(C–O): 1282 cm^{-1}.

Strain and growth conditions

Strain and growth conditions. A fresh *C. tropicalis* clinical isolate was isolated and characterized by the Central Public Health Laboratory (LACEN-BA). The resultant strain (Ct-LACEN 201103) was used here. Cultures were carried out in 4% potato dextrose agar solid medium and in RPMI 1640 liquid medium buffered with MOPS (3 acid [N-morpholino] propane sulfonic) pH 7.0, at 35 °C. *C. tropicalis* proliferation was determined daily under phase-microscopy on hemocytometric chambers and IC_{50} determined using GraphPad Prism 5.01. *C. tropicalis* viability was assessed by colony-forming unit (CFU) counting.

Cytotoxicity Assays

Splenocytes from 8-10 weeks-old BALB/c mice were incubated in 24-well culture plates at 37 °C, 5%CO_2 in RPMI supplemented with 10% fetal bovine serum (Sigma-Aldrich), with 125, 250, 500 and 1000 µM RuCat for 24h. After incubation, 5 mg mL^{-1} MTT in phosphate-buffered saline (PBS) were added for 2h, then DMSO was added to dissolve the formazan crystals and absorbance values were determined at 540 nm. EC_{50} was determined using GraphPad Prism 5.01.

Propidium iodide staining

C. tropicalis treated with 40µM RuCat for 1 h at 35 °C in RPMI 1640 were incubated with 10 µg/mL propidium iodide (PI - Sigma Chemical Co. St. Louis Mo USA) for 5 min. Acquisition was performed using a BD FACSCalibur™ flow cytometer and data were analyzed in BD CellQuest™ software (San Jose, CA).

Fluorescence microscopy for detection of reactive species

For detection of ROS, yeasts were cultured in the presence and absence of 38 µM RuCat for 60 min. Then the cells were washed in PBS, stained with 10 µM of the fluorescent probe 2',7'-dichlorodihydrofluorescein diacetate (H_2DCFDA) (Molecular Probes, Eugene, OR) for 30 min and observed in a Olympus BX51 fluorescence microscope at 460 to 495nm. 5 mM H_2O_2 were used for 1 hour as a positive control, and 5 mM ascorbic acid 2h pretreatments, prior to H_2O_2, as negative control. The fluorescence was detected by using excitation and emission spectra of 495 nm and 529 nm.

Evaluation of Lipid Peroxidation

After treatment with 24, 70 and 140 µM RuCat for 1h, the samples were washed in PBS, 200 µL of thiobarbituric acid (1%) were added and diluted with 50% acetic acid. Then the samples were incubated at 100 °C for 2h and the reaction was stopped in ice bath for 15 min. Thiobarbituric acid reactive substances (TBARS) were measured by spectrophotometry at 532 nm.

Cell Wall Staining

Yeast cells treated with 70 and 140 µM RuCat for 2 h were washed in PBS, stained with 30 µg mL^{-1} Calcofluor White (CW - MP Biomedicals) and observed at 355 nm in a Olympus BX51 fluorescence microscope.

Transmission Electron Microscopy (TEM).

Cells were fixed in 2.5% glutaraldehyde and 4% paraformaldehyde in 0.1 M sodium cacodylate buffer, pH 7.4 and post-fixed in 1.5% of potassium permanganate for 1h,

protected from light (Vannier-Santos and Lins 2001). Samples were dehydrated in acetone series and imbed in Spurr's resin (Ted Pella, Redding, CA). Ultrathin sections were, collected on 300-mesh cooper grids, contrasted in 5% uranyl acetate and 3% lead citrate. The ultrastructural analysis was performed on a Zeiss109 transmission electron microscope at 80 kV.

Scanning Electron Microscopy (SEM). Yeast cells were fixed and dehydrated as above, followed by critical point drying and gold metallization and observation in JEOL JSM 6390 scanning electron microscope at 20kV (Vannier-Santos and De Castro 2009).

Statistical Analysis

Data represent the mean and standard deviation, of three independent experiments and statistical analysis was performed employing ANOVA and Dunnett's post-test with $p < 0.05$, using GraphPad Prism 5.01.

Ethical Aspects

All the procedures performed were approved by the Fiocruz Ethics Committee (lic. no. 20/2015) and followed the ethics standards guidelines of International Council for Laboratory Animal Science.

RESULTS

Effect of RuCat on *C. tropicalis* proliferation

RuCat incubation significantly (p <0.05) inhibited the growth of fluconazole-resistant *C. tropicalis*, in RPMI 1640 for 24h at 35 °C, from 20 µM, dose-dependently. The obtained RuCat IC_{50} was 20.3 µM (Figure 1A).

Cytotoxicity evaluation of RuCat in splenocytes cultures

In order to determine the RuCat effects on mammalian cells, MTT cytotoxicity assays using Balb/c splenocytes were performed. Splenocyte cultures incubated with different concentrations of the compound for 24 h showed significant toxicity only at concentrations of 500 and 1000 µM (Figure 1B) and the obtained EC_{50} was 325 µM.

Cell Surface Analysis

We used SEM to analyze the possible RuCat effects upon fluconazole-resistant *C. tropicalis* incubated with 9, 18, 38 µM of the compound for 24 h (Figure 2). Untreated control samples showed numerous ovoid yeast with smooth, continuous surfaces (Figure 2 A, B); Cultures treated with 9 µM RuCat presented remarkable pseudohyphae formation (Figure 2 C, D). Cultures incubated with 18 µM RuCat displayed intense cellular aggregation (Figure 2 E) and higher magnifications revealed the presence of

surface cracks (Figure 2 F), whereas cultures incubated with 38 µM cells showed scarce cells and large amount of cellular debris (Figure 2 G, H).

Necrosis Detection

In order to verify whether RuCat caused *C. tropicalis* necrosis, cultures were incubated with PI to test membrane discontinuity assessed by flow cytometry. Contrary to untreated controls, after 1 hour of treatment with 40 µM RuCat we found 30% of the population was PI-labeled (Suppl. Fig. 2).

Evaluation of ROS formation

The probe 2',7'-dichlorofluorescein diacetate (H_2DCFDA) was employed to detect the ROS production caused by 38 µM RuCat for 1h (Figure 3). Untreated control cells were unlabeled (Fig. 3A, B). The positive control incubated with 5 mM H_2O_2 for 1h showed positive reaction (Figure 3C, D), which was completely reversed by 5 mM ascorbic acid preincubation (Figure 3E, F). RuCat treatment resulted in intense H_2DCFDA labeling (G, H) which was partially reverted by ascorbic acid preincubation (I, J).

In order to evaluate the enhanced ROS production-induced oxidative stress we measured lipoperoxidation in RuCat-treated yeasts.

Oxidative Stress Role in the RuCat Anti-*Candida tropicalis* Action

The measurement of TBARS was employed evaluate oxidative stress changes indicated by lipid peroxidation. Increased ROS production led to enhanced lipoperoxidation and presumably membrane damage. We measured TBARS formation after 1h exposure to different RuCat concentrations (24, 70 and 140 µM). The concentrations tested significantly (p <0.05) increased lipoperoxidation (Figure 4A).

In order to test the possible participation of the oxidative stress in the RuCat anti-*Candida* activity, we preincubated cultures with 20 mM N-acetyl-*L*-cysteine (NAC) for 2 h before treatment with 150 µM RuCat. CFU counting was performed after 24h. We notice that NAC completely restored the viability of these cells reverting the RuCat activity (Figure 4B).

Candida tropicalis cell wall staining

The CW chitin-binding probe was used for labeling *C. tropicalis* cell walls to assess the integrity of the cell surfaces, after treatment with RuCat for 2h. Untreated yeasts were intensely labeled with CW (Figure 5 A, B), whereas fungal cells treated with 70 µM (Figure 5C, D) or 140 µM RuCat (Figure 5E, F) were weakly labeled.

In order to approach the RuCat-induced mechanism of yeasts cell death we evaluated the ultrastructural changes caused by 40 and 60 µM RuCat for 3h and 24 h. Untreated control yeasts displayed intact and regular cell wall structure, polymorphic nuclei and well-preserved mitochondria (Figure 6A), whereas RuCat-treated cells showed vesicular compartments with different amounts of amorphous electrondense material (Figure 6B, C), as well as melanin granules in membrane-bounded organelles (Figure 6D), periplasmic region and covering the external cell surface (Figure 6B) and free in the extracellular milieu (Figure 6 C-E). Surface adherent membrane fragments (Figure 6 C, D) were also observed.

DISCUSSION

In plants catechol oxidation provides a natural protection against infections via ROS production (Kumar and Pandey 2013). Its pro-oxidant effect may result from an auto-oxidation in aqueous solution and physiological pH, leading to the formation of quinone and superoxide radicals which are highly cytotoxic (O'Brien 1991). ROS production may account at least in part for the SEM alterations and H_2DCFDA staining. CW labelling could also be precluded by melanin and or membrane fragments lining fungal cell surfaces.

The high instability of catechol in aqueous solution, can be blocked by ruthenium (III) ion binding via coordination linked in the oxygen atom producing RuCat causing stability in aqueous solution for at least one week (de Lima *et al.* 2004). It was previously reported that the combination of the ruthenium (III) and catecholamine ligands led to fungicidal activity significantly higher than free ligands due to metal ion playing an important role in the action of the complex on *Candida* sp. (de Lima *et al.* 2003).

Determination of RuCat Selectivity Index comparing RuCat effects on *C. tropicalis* and murine splenocytes *in vitro* [IS= CC_{50} (325 µM)/EC_{50} (20.3 µM)], may be indicative of a promising agent as IS should be over 10-fold (Nwaka *et al.* 2009) and the IS value obtained here was 16.

Ultrastructural analysis showed that treatment of *C. tropicalis* yeasts with RuCat increased melanin granules, trafficking in vesicles to the fungal surface and release to extracellular milieu. *C. albicans* was shown to produce and externalize melanin both *in vitro* and *in vivo* (Morris-Jones *et al.* 2005). Melanin is a generic term for a heterogeneous class of natural pigments widely present in mammals, protozoa, plants, fungi and bacteria with a multitude of biological functions. The production of melanin

by fungi is of fundamental importance, comprising a relevant virulence factor for several species. In fungi the final destination of melanin is the cell wall, which can be found within the wall itself or as a layer in the periplasmic space (Langfelder *et al.* 2003), contributing to their protection against oxidative damage caused by phagocytes, antifungal substances action among other stress conditions (van Duin *et al*. 2002; Gómez and Nosanchuk, 2003; Nosanchuk and Casadevall 2006).

Previous studies have reported the presence of melanin granules located in the cytoplasm similarly to mammalian melanosomes (*e.g. Cladosporium carrionii* and *Fonsecaea pedrosoi*) (San-Blas *et al.* 1996; Franzen *et al.* 2008) and indicating a possible association between melanin production and chitin synthesis (Walker *et al.* 2010). The membrane-bounded compartments detected by TEM may comprise fungal melanosomes that are transported to the cell periphery, where melanin granules are transferred to the cell wall (Nosanchuk *et al*. 2015). Although the mechanism of melanin externalization has not yet been fully established the export process probably involves the chitinase genes (*CHT2* and *CHT3*) and the chitin regulatory pathway suggesting association between cell surface disruption seen by SEM (Walker *et al.* 2010). Part of the granular material observed by SEM in 38 µM RuCat-treated cells may be due to melanin, as these structures were previously described by electron microscopy (Walker *et al.* 2010).

There is a wide variety of biological reactions which underlie the RuCat toxicity and the ruthenium combination is possibly implicated in the ROS production and its deleterious effect (Almeida *et al.* 2007). The oxidation of RuCat in the presence of oxygen leads to the formation of superoxide radical ($O_2^{\bullet-}$) and melanin may exert antioxidant effect quenching free radicals (Fernandes *et al.* 2015). Interestingly

catecholamine precursors are involved in *Cryptococcus neoformans* melanization (Chatterjee *et al.* 2012).

The RuCat treatment presumably triggered the antioxidant defense system for detoxification of $O_2^{\bullet-}$ into H_2O_2 by the cytoplasmic enzyme superoxide dismutase (SOD). Then H_2O_2 is converted by catalase into water and oxygen, however, formation of such ROS may exceed its protection capacity resulting in the oxidative stress reported here. The pseudohyphal development and aggregation phenotypes observed maybe related to oxidant stress adaptation (Boisnard *et al.* 2008).

Taken together the present data indicate that RuCat may comprise useful tools in the development of fungicidal agents.

Acknowledgments

The authors acknowledge LACEN for providing the fungal isolate.

Funding

Supported by the Conselho Nacional de Desenvolvimento Científico e Tecnológico (CNPq/PROEP); Coordenação de Aperfeiçoamento de Pessoal de Nível Superior (Capes/PROCAD); Fundação de Amparo à Pesquisa do Estado da Bahia (FAPESB); Programa Pesquisa para o Sistema Único de Saúde (PPSUS) and FIOCRUZ MAVS is a CNPq research fellow.

Conflict of interest: None declared.

5. REFERENCES

Almeida WLC, Vítor DN, Pereira MRG *et al.* Redox properties of ruthenium complex with catechol are involved in toxicity to glial cells. *J Chil Chem Soc* 2007; **52**: 1240–3.

Boisnard S, Ruprich-Robert G, Florent M *et al.* Role of Sho1p adaptor in the pseudohyphal development, drugs sensitivity, osmotolerance and oxidant stress adaptationin the opportunistic yeast *Candida lusitaniae*. *Yeast* 2008; **25**: 849–59.

Cantón E, Viudes A, Pemán J. Systemic nosocomial infection by yeasts. *Rev Iberoam Micol* 2001; **18**: 51–5.

Canuto MM, Rodero FG. Antifungal drug resistance to azoles and polyenes. *Lancet Infect Dis* 2002; **2**: 550–63.

Chatterjee S, Prados-Rosales R, Frases S *et al.* Using solid-state NMR to monitor the molecular consequences of Cryptococcus neoformans melanization with different catecholamine precursors. *Biochemistry* 2012; **51**: 6080–8.

Colombo AL, Guimarães T. Epidemiologia das infecções hematogênicas por *Candida* spp. *Rev Soc Bras Med Trop* 2003; **36**: 599–607.

van Duin D, Casadevall A, Nosanchuk JD. Melanization of *Cryptococcus neoformans* and Histoplasma capsulatum reduces their susceptibilities to amphotericin B and caspofungin. *Antimicrob Agents Chemother* 2002; **46**: 3394–400.

Fernandes C, Prados-Rosales R, Silva B *et al.* Activation of melanin synthesis in Alternaria infectoria by antifungal drugs. *Antimicrob Agents Chemother* 2015; **60**: 1646-55.

Franzen AJ, Cunha MML, Miranda K *et al.* Ultrastructural characterization of melanosomes of the human pathogenic fungus *Fonsecaea pedrosoi*. *J Struct Biol* 2008; **162**: 75–84.

Fuentes M, Hernández R, Gordillo D *et al.* Antifungal activity of melanin in clinical isolates of *Candida* spp. *Rev Chil infectología* 2014; **31**: 28–33.

García-Rodríguez J, Cantón E, Pemán J *et al.* Age group, geographical incidence and patterns of antifungal susceptibility of *Candida* species causing candidemia in the Spanish paediatric population. *Enferm Infecc Microbiol Clin* 2013; **31**: 363–8.

Ghannoum MA. *Candida*: a causative agent of an emerging infection. *J Investig Dermatol Symp Proc* 2001; **6**: 188–96.

Gómez BL, Nosanchuk JD. Melanin and fungi. *Curr Opin Infect Dis* 2003; **16**: 91–6.

Gudlaugsson O, Gillespie S, Lee K *et al.* Attributable mortality of nosocomial candidemia, revisited. *Clin Infect Dis* 2003; **37**: 1172–7.

Kocac Ismail Alıskan, Ismet Talan IT. Antimicrobial Activity of Catechol and Pyrogallol as

Allelochemicals. *Z Naturforsch* 2006; **61c**: 639–42.

Kumar S, Pandey AK. Chemistry and biological activities of flavonoids: an overview. *Sci World J* 2013; **2013**: 162750.

Langfelder K, Streibel M, Jahn B *et al.* Biosynthesis of fungal melanins and their importance for human pathogenic fungi. *Fungal Genet Biol* 2003; **38**: 143–58.

de Lima RG, Lever ABP, Ito IY *et al.* Antifungal activity of novel catecholamine ruthenium(III) complexes. *Transit Met Chem* 2003; **28**: 272–5.

de Lima RG, Marchesi MSP, de Godoy MAF *et al.* Structure-activity relationship of coordinated catecholamine in the [Ru(III)(NH3)4(catecholamine)]+ complex. *Int J Pharm* 2004; **271**: 21–30.

Melo NR, Taguchi H, Jorge J *et al.* Oral Candida flora from Brazilian human immunodeficiency virus-infected patients in the highly active antiretroviral therapy era. *Mem Inst Oswaldo Cruz* 2004; **99**: 425–31.

Morace G, Borghi E, Iatta R *et al.* Antifungal susceptibility of invasive yeast isolates in Italy: the GISIA3 study in critically ill patients. *BMC Infect Dis* 2011; **11**: 130.

Moran, G; Coleman, D.; Sullivan D. An Introduction to the Medically Important *Candida* Species. *In*: Calderone R A and Clancy C J (Eds). *Candida and Candidiasis*, *Second Edition*. American Society of Microbiology, 2012, 11–25.

Morris-Jones R, Gomez BL, Diez S *et al.* Synthesis of melanin pigment by *Candida albicans* in vitro and during infection. *Infect Immun* 2005; **73**: 6147–50.

Nosanchuk JD, Casadevall A. Impact of melanin on microbial virulence and clinical resistance to antimicrobial compounds. *Antimicrob Agents Chemother* 2006; **50**: 3519–28.

Nosanchuk JD, Stark RE, Casadevall A. Fungal Melanin: What do We Know About Structure? *Front Microbiol* 2015; **6**: 1463.

Nucci M, Queiroz-Telles F, Tobón AM *et al.* Epidemiology of opportunistic fungal infections in Latin America. *Clin Infect Dis* 2010; **51**: 561–70.

Nunn MA, Schäfer SM, Petrou MA *et al.* Environmental source of *Candida dubliniensis*. *Emerg Infect Dis* 2007; **13**: 747–50.

Nwaka S, Ramirez B, Brun R *et al.* Advancing drug innovation for neglected diseases-criteria for lead progression. *PLoS Negl Trop Dis* 2009; **3**: e440.

O'Brien PJ. Molecular mechanisms of quinone cytotoxicity. *Chem Biol Interact* 1991; **80**: 1–41.

Oliveira VKP, Ruiz L da S, Oliveira NAJ *et al.* Fungemia caused by *Candida* species in a children's public hospital in the city of São Paulo, Brazil: study in the period 2007-2010. *Rev Inst Med Trop São Paulo* 2014; **56**: 301–5.

Ruiz LS, Sugizaki MF, Montelli AC *et al.* Fungemia by yeasts in Brazil: Occurrence and phenotypic study of strains isolated at the Public Hospital, Botucatu, São Paulo. *J Mycol Med* 2005; **15**: 13–21.

San-Blas G, Guanipa O, Moreno B *et al. Cladosporium carrionii* and *Hormoconis resinae* (*C. resinae*): Cell wall and melanin studies. *Curr Microbiol* 1996; **32**: 11–6.

Santana da Silva R, Gorelsky SI, Dodsworth ES *et al.* Synthesis, spectral and redox properties of tetraammine dioxolene ruthenium complexes. *J Chem Soc Dalt Trans* 2000; 4078–88.

Schweigert N, Zehnder AJB, Eggen RIL. Chemical properties of catechols and their molecular modes of toxic action in cells, from microorganisms to mammals. *Environ Microbiol* 2001; **3**: 81–91.

Takahashi K, Kita E, Konishi M *et al.* Translocation model of *Candida albicans* in DBA-2/J mice with protein calorie malnutrition mimics hematogenous candidiasis in humans. *Microb Pathog* 2003; **35**: 179–87.

Tapia C V, Falconer M, Tempio F *et al.* Melanocytes and melanin represent a first line of innate immunity against *Candida albicans*. *Med Mycol* 2014; **52**: 445–54.

Vannier-Santos MA, De Castro SL. Electron microscopy in antiparasitic chemotherapy: a (close) view to a kill. *Curr Drug Targets* 2009; **10**: 246–60.

Vannier-Santos MA, Lins U. Cytochemical techniques and energy-filtering transmission electron microscopy applied to the study of parasitic protozoa. *Biol Proced Online* 2001; **3**:

8–18.

Walker CA, Gómez BL, Mora-Montes HM *et al.* Melanin externalization in *Candida albicans* depends on cell wall chitin structures. *Eukaryot Cell* 2010; **9**: 1329–42.

Warnock DW. Trends in the epidemiology of invasive fungal infections. *Jpn J Med Mycol* 2007; **48**: 1-12.

Figure 1: Antifungal activity of different concentrations of RuCat on fluconazole-resistant *C. tropicalis* strain, determined by cell counting in RPMI 1640 for 24h at 35 °C (A); MTT activity of Balb/c mice splenocytes treated *in vitro* with different RuCat concentrations in RPMI-1640 medium containing 10% fetal calf serum (B). Data are representative of at least three independent experiments, expressed as means plus standard deviations and analyzed using ANOVA and Dunnett's post-test. * $p < 0.05$.

Figure 2: Scanning electron microscopy of fluconazole-resistant *C. tropicalis*, comparing untreated control cells (A, B) and cultures incubated with 9 (C, D), 18 (E, F) and 38 (G, H) µM RuCat for 24 h. Control cells showed a normal oblong shape (A, B) whereas cultures treated with 9 µM and 18 µM showed, respectively, the profuse formation of pseudohyphae (C, D) and cell aggregation (E, F). At higher magnifications, fractured cell surfaces were observed (F, arrows). In preparations incubated with 38 µM (G and H) a marked a reduction in yeast cell numbers was observed (G), as well as disrupted cells (arrow) and large amount of cellular debris (arrowheads).

Figure 3: ROS formation in fluconazole-resistant *C. tropicalis* detected using the probe H_2DCFDA. Untreated control yeasts were unlabeled (A and B) whereas yeasts treated with 5 mM H_2O_2 (C and D) for 60 min, showed green fluorescence, which was completely reverted by two hours pre-incubation with 5 mM ascorbic acid (E and F).

Fungal cells treated with 38 µM RuCat for 60 min displayed intense H_2DCFDA labeling (G and H), which was partially reverted by 5 mM ascorbic acid pretreatment (I, J). Bars represent 50 µm.

Figure 4: RuCat for 1h significantly and dose-dependently enhanced lipid peroxidation in fluconazole-resistant *C. tropicalis* accessed by thiobarbituric acid-reacting substances (TBARS) measurements (A). RuCat-induced *C. tropicalis* impaired proliferation was reverted by 20 mM N-acetyl-*L*-cysteine (NAC) preincubation. Cell densities (A) and CFU counts (B) determined after 24 h are representative of at least three independent replicates. Data expressed as means ± standard deviations were analyzed using ANOVA and Dunnett's post-test, $*p < 0.05$.

Figure 5: *C. tropicalis* yeast cell walls chitin staining using 30 µg mL^{-1} calcofluor white for 2h. Control yeast cells (A, B) were intensely stained, whereas cells treated with 70 µM (C, D) and 140 µM (E, F) RuCat presented weak or no labelling. Bars represent 50 µm.

Figure 6: Transmission electron microscopy of fluconazole-resistant *C. tropicalis*, untreated control cells (A) and yeasts grown with 40 µM (B, E) or 60 µM (C, D) RuCat for 3 h and 6h, respectively. Untreated yeasts presented a well-preserved cell architecture, with regular cell wall with subjacent plasma membrane, nucleus (n), mitochondria (m). However, in treated yeasts (B-E), vesicular compartments with varied amounts of electrondense material were observed (B, C *). Melanin granules were observed within membrane-bounded vesicles (D, arrowhead), in the periplasmic space (D, E white arrows) and outside the fungal cell walls (B, E black arrows). Besides extracellular melanin granules (C, arrowheads), membrane fragments (C, D, black arrows) were observed adherent to the surface of RuCat-treated yeasts (C, arrows).

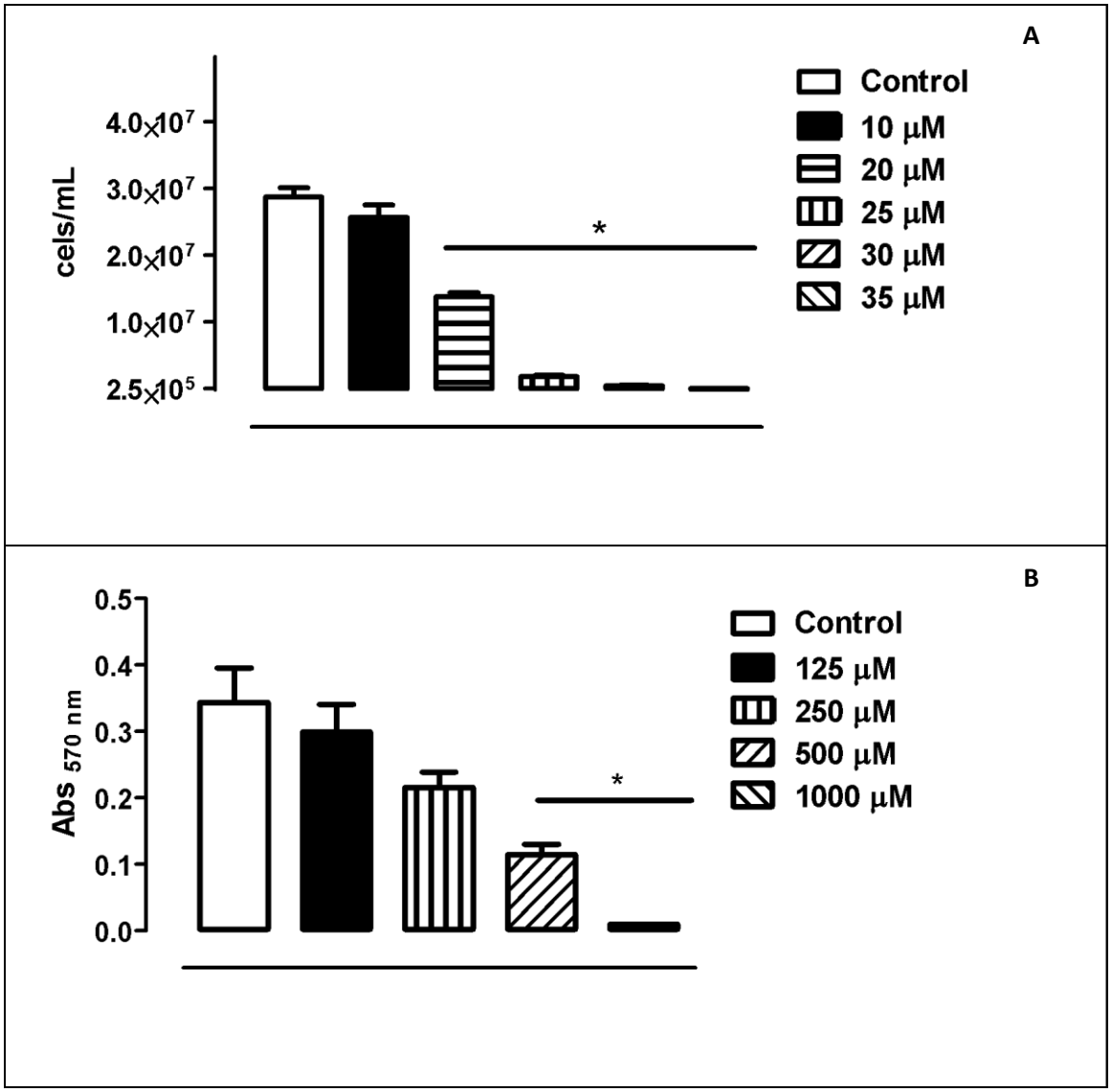

Figure 1: Antifungal activity of different concentrations of RuCat on fluconazole-resistant *C. tropicalis* strain, determined by cell counting in RPMI 1640 for 24h at 35 °C (A); MTT activity of Balb/c mice splenocytes treated *in vitro* with different RuCat concentrations in RPMI-1640 medium containing 10% fetal calf serum (B). Data are representative of at least three independent experiments, expressed as means plus standard deviations and analyzed using ANOVA and Dunnett's post-test. * p <0.05.

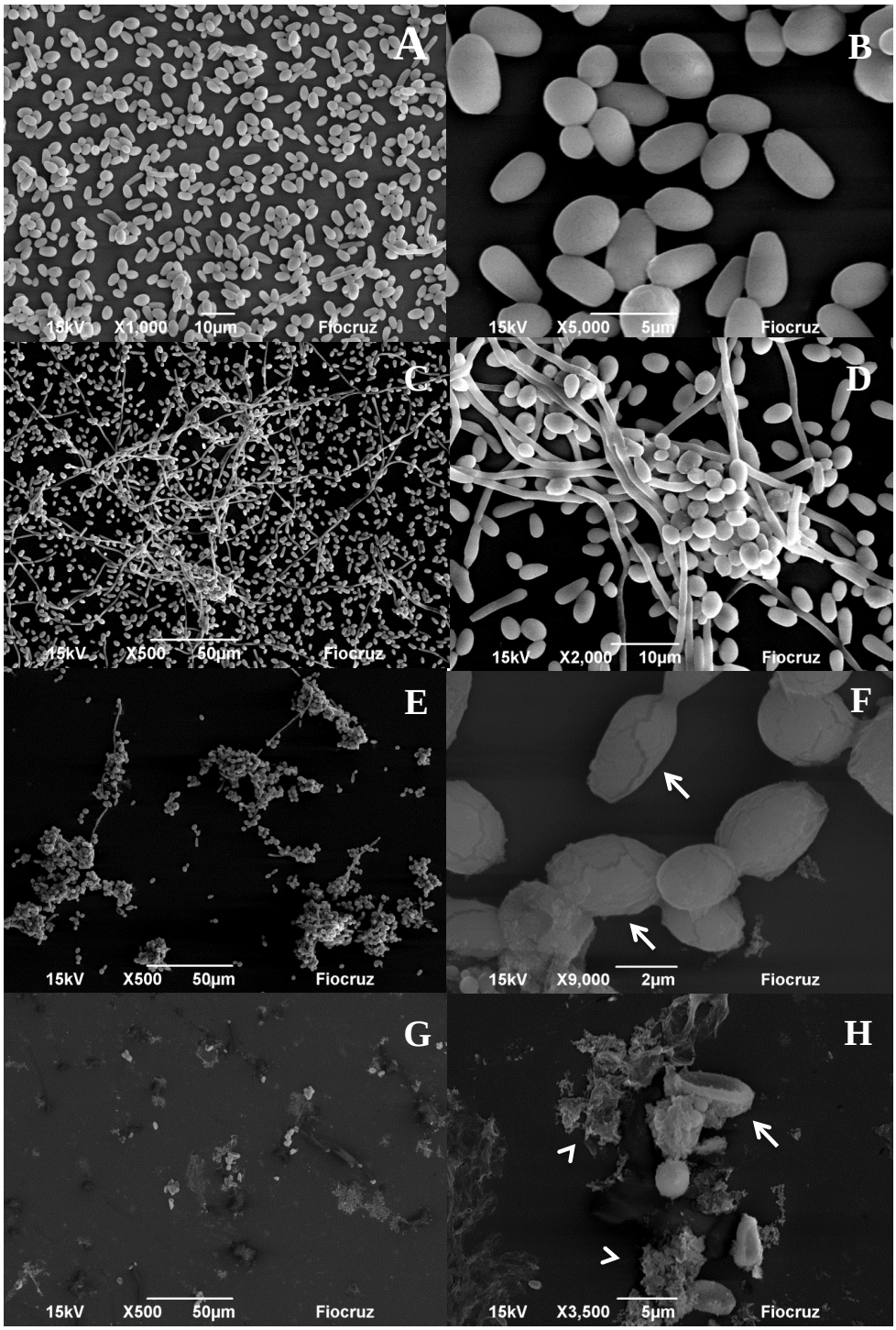

Figure 2: Scanning electron microscopy of fluconazole-resistant *C. tropicalis*, comparing untreated control cells (A, B) and cultures incubated with 9 (C, D), 18 (E, F) and 38 (G, H) µM RuCat for 24 h. Control cells showed a normal oblong shape (A, B) whereas cultures treated with 9 µM and 18 µM showed, respectively, the profuse formation of pseudohyphae (C, D) and cell aggregation (E, F). At higher magnifications, fractured cell surfaces were observed (F, arrows). In preparations incubated with 38 µM (G and H) a marked a reduction in yeast cell numbers was observed (G), as well as disrupted cells (arrow) and large amount of cellular debris (arrowheads).

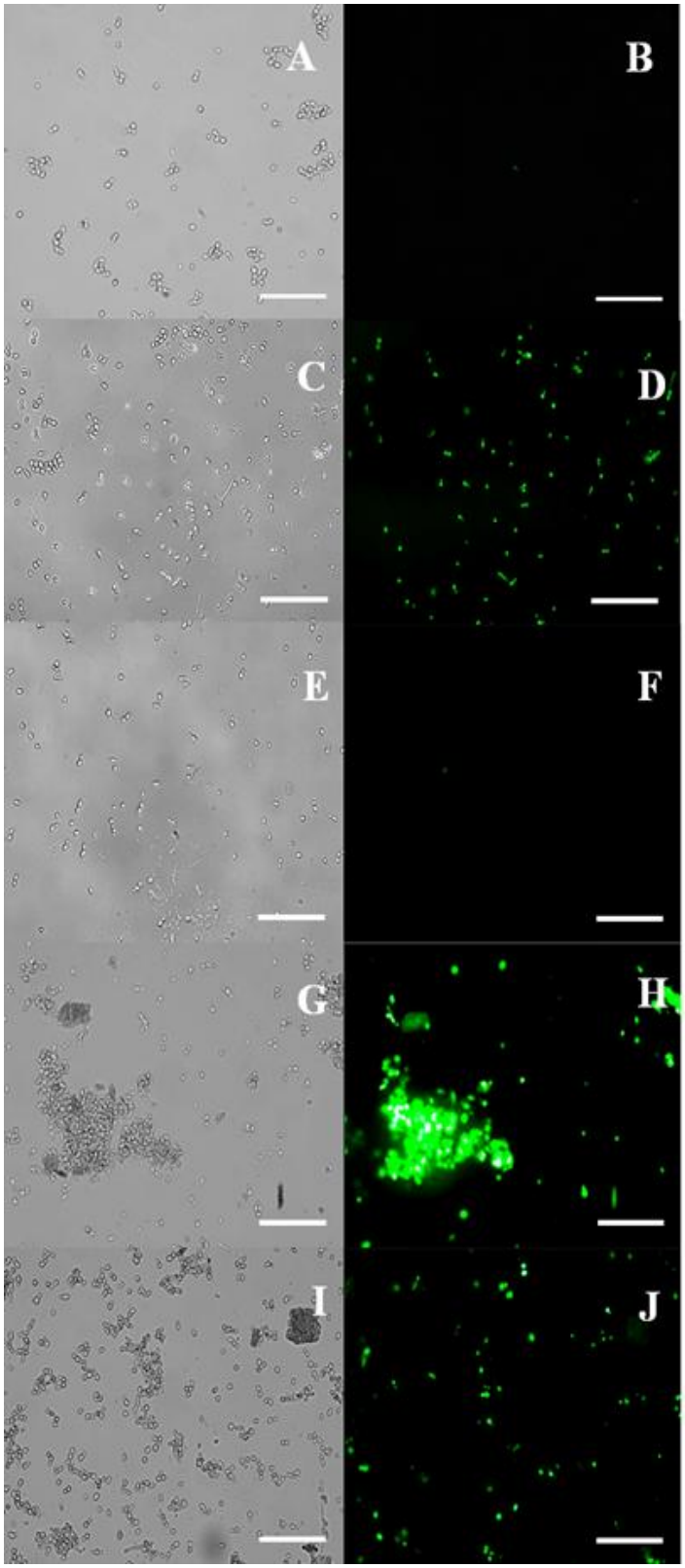

Figure 3: ROS formation in fluconazole-resistant *C. tropicalis* detected using the probe H_2DCFDA. Untreated control yeasts were unlabeled (A and B) whereas yeasts treated with 5 mM H_2O_2 (C and D) for 60 min, showed green fluorescence, which was completely reverted by two hours pre-incubation with 5 mM ascorbic

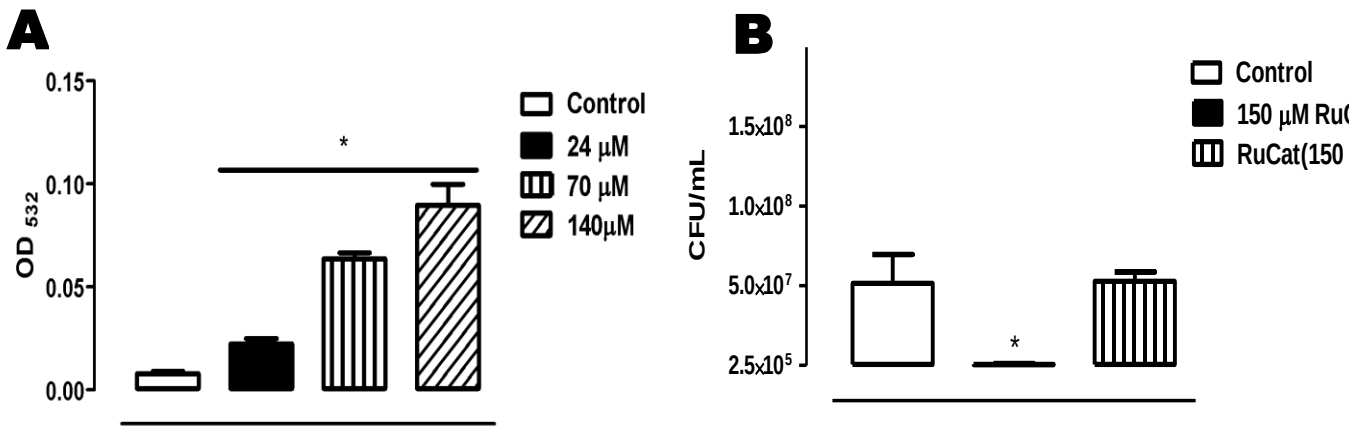

Figure 4: RuCat for 1h significantly and dose-dependently enhanced lipid peroxidation in fluconazole-resistant *C. tropicalis* accessed by thiobarbituric acid-reacting substances (TBARS) measurements (A). RuCat-induced *C. tropicalis* impaired proliferation was reverted by 20 mM N-acetyl-*L*-cysteine (NAC) preincubation. Cell densities (A) and CFU counts (B) determined after 24 h are representative of at least three independent replicates. Data expressed as means ± standard deviations were analyzed using ANOVA and Dunnett post-test, **p* <0.05.

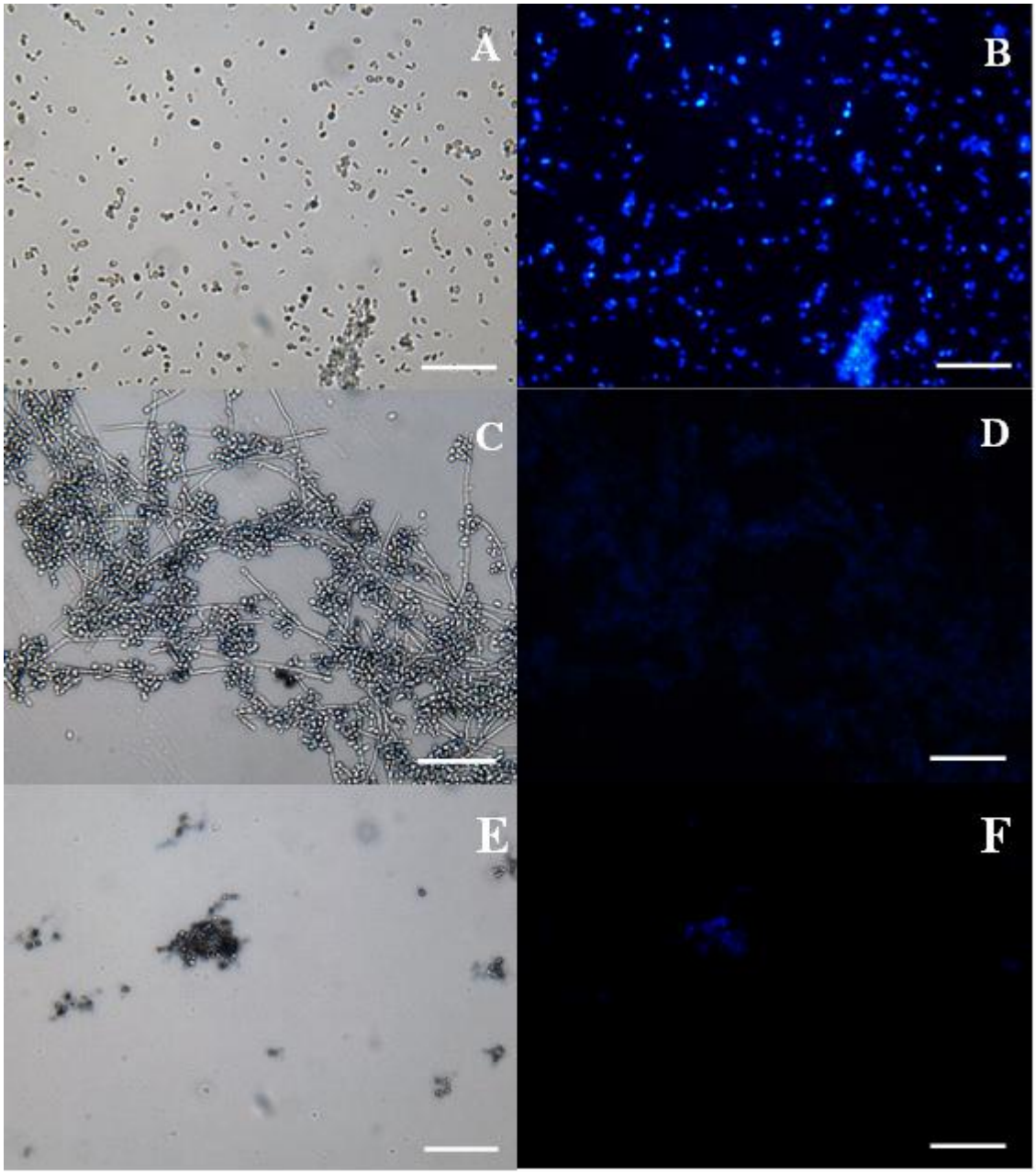

Figure 5: *C. tropicalis* yeast cell walls chitin staining using 30 µg mL^{-1} calcofluor white for 2h. Control yeast cells (A, B) were intensely stained, whereas cells treated with 70 µM (C, D) and 140 µM (E, F) RuCat presented weak or no labelling. Bars represent 50 µm.

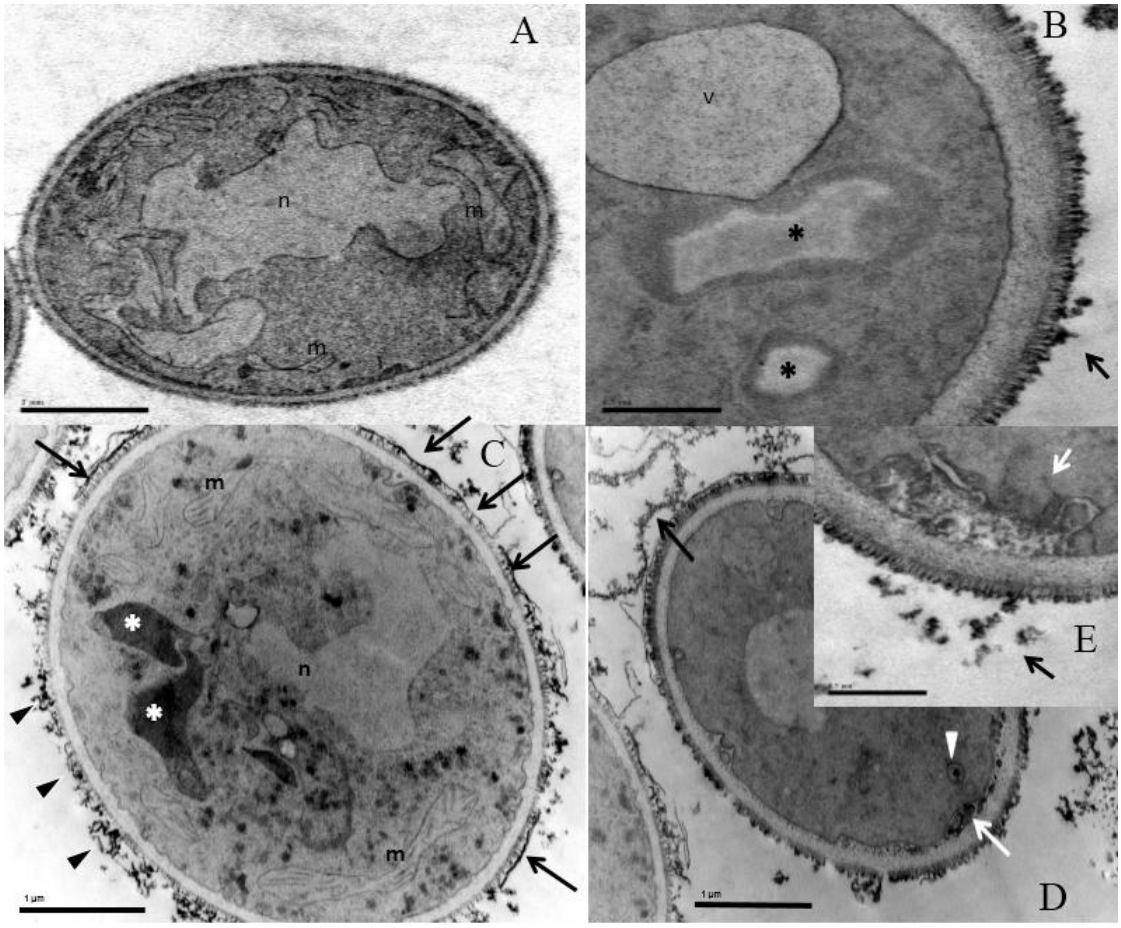

Figure 6: Transmission electron microscopy of fluconazole-resistant *C. tropicalis*, untreated control cells (A) and yeasts grown with 40 µM (B, E) or 60 µM (C, D) RuCat for 3 h and 6h, respectively. Untreated yeasts presented a well-preserved cell architecture, with regular cell wall with subjacent plasma membrane, nucleus (n), mitochondria (m). However, in treated yeasts (B-E), vesicular compartments with varied amounts of electrondense material were observed (B, C *). Melanin granules were observed within membrane-bounded vesicles (D, arrowhead), in the periplasmic space (D, E white arrows) and outside the fungal cell walls (B, E black arrows). Besides extracellular melanin granules (C, arrowheads), membrane fragments (C, D, black arrows) were observed adherent to the surface of RuCat-treated yeasts (C, arrows).